A multi-timescale modeling methodology for PEMFC performance and durability in a virtual fuel cell car

Manik Mayur*[a], Stephan Strahl[b], Attila Husar[b], Wolfgang G. Bessler[a]

[a]Institute of Energy System Technology (INES), Offenburg University of Applied Sciences, Badstr. 24, 77654 Offenburg, Germany

[b]Institut de Robòtica i Informàtica Industrial (CSIC-UPC), Parc Tecnològic de Barcelona, C/Llorens i Artigas 4-6, 08028 Barcelona, Spain

*Corresponding author

Email: manik.mayur@hs-offenburg.de, Tel: +49 781 2054755

Abstract.

The durability of polymer electrolyte membrane fuel cells (PEMFC) is governed by a nonlinear coupling between system demand, component behavior, and physicochemical degradation mechanisms, occurring on timescales from the sub-second to the thousand-hour. We present a simulation methodology for assessing performance and durability of a PEMFC under automotive driving cycles. The simulation framework consists of (a) a fuel cell car model converting velocity to cell power demand, (b) a 2D multiphysics cell model, (c) a flexible degradation library template that can accommodate physically-based component-wise degradation mechanisms, and (d) a time-upscaling methodology for extrapolating degradation during a representative load cycle to multiple cycles. The computational framework describes three different time scales, (1) sub-second timescale of electrochemistry, (2) minute-timescale of driving cycles, and (3) thousand-hour-timescale of cell ageing. We demonstrate an exemplary PEMFC durability analysis due to membrane degradation under a highly transient loading of the New European Driving Cycle (NEDC).

Keywords: Polymer Electrolyte Membrane Fuel Cell (PEMFC); Modeling; Virtual car; Degradation

1 Introduction

Polymer electrolyte membrane fuel cells (PEMFC) can provide rapid (sub-second) load transients, which is particularly useful for providing power to electrically-powered automobiles [1]. However, it has been shown that rapid load changes and persistent open circuit voltage (OCV) operations cause accelerated degradation of the PEMFC components [2]. Therefore, in practice, PEMFC stacks for electric vehicles are today hybridized with high-power batteries or supercapacitors that provide fast power response, while the PEMFC is operated under near-constant load. Chan et al. reviewed the current trends in the vehicle modeling of electric, hybrid and fuel cell cars [3]. Jiang et al. carried out control studies in a hybrid fuel cell and battery source under pulsed loading [4]. Thounthong et. al. studied the energy management [5] and control [6] of fuel cell, battery, and supercapacitor hybrid for vehicle application. Using a hybrid arrangement increases PEMFC lifetime, while increasing system cost, weight and complexity. In the present work, we therefore study PEMFCs for fully transient car operation without hybridization. In this case, the fuel cell stack is exposed to a highly non-periodic power demand.

One of the major bottlenecks to the commercialization of non-hybrid fuel cell vehicles is durability of a fuel cell stack that indirectly increases the cost [7]. Borup *et. al.* [8] gave an overview of component-wise degradation mechanisms and testing procedures to understand component wise fuel cell durability. Similarly, considerable research has been carried out on the transient loading of fuel cells with respect to cell aging and degradation, and most of them focus on the cell component-wise degradation at nominal fuel cell operating conditions or simulated periodic load cycling [9–11]. In order to understand the degradation mechanisms and their functional dependence on transient operating conditions, a systematic approach towards understanding the complex multiscale transport and reactions inside the PEMFCs is required. Multiphysics modeling is an excellent tool to unravel the complex and nonlinear interactions between performance, degradation, cell design, and operating conditions [12–14]. In particular, virtual cells can be calibrated using experiments under well-defined operating conditions and then be studied under more realistic automotive load profiles.

In this study we expand upon state-of-the-art fuel cell vehicle modeling approaches [15–21] by coupling a system model with a detailed multiphysics single-cell model [22]. We introduce a multi-methodology modeling and simulation approach for PEMFC performance and durability over realistic driving cycles and complete cell lifetime. The approach covers multiple interacting systems (electric car, single cell with components, detailed electrochemical transport and kinetics) and multiple time scales (single-cell behavior on sub-second scale, driving cycle on 20 minute scale, cell lifetime on 5.000 hour scale). In the present study, the virtual fuel cell car is assumed to operate on the new European driving cycle (NEDC) used for regulating vehicle emissions and fuel economy in passenger cars [23]. The velocity demand from the driving cycle is converted into a power demand using a system-level model of an electric car governed by a force balance and Newton's laws of motion. The fuel cell itself is modeled by using a multiphysics approach. Multi-species transport of fuel, air and water vapor in the gas channels, diffusion layers and the polymer membrane are described with the help of computational fluid dynamics (CFD) over the two-dimensional (2D) cell geometry. The electrochemical kinetics of oxygen reduction in the catalyst layer is derived from elementary reaction steps and is implemented in a modified Butler-Volmer formalism. Due to high computational demand of transient simulations, we further introduce a method of time-upscaling by extrapolating degradation over a single drive cycle over multiple consecutive cycles. As a result, the complete lifetime of a PEMFC under transient operating conditions can be assessed. The fuel cell behavior is analyzed in terms of dynamic current and voltage behavior as well as water management.

2 Simulation framework

2.1 Overview and model assumptions

Figure 1 shows the four basic components of the present simulation methodology, that is, (a) a 0D system model of a fuel cell car including fuel cell stack, electric engine, power train, force balance, and engine controller; (b) a 2D multiphysics CFD model of a single cell including transport in channels, gas diffusion layers (GDL) and membrane as well as electrochemistry; (c) a library of degradation mechanisms that can be filled and validated independently of the present framework; (d) a meth-

odology for time-upscaling of degradation over the complete fuel cell lifetime; and (e) on-the-fly coupling of all components for full-scale dynamic simulations. The components will be described in detail in the following sections.

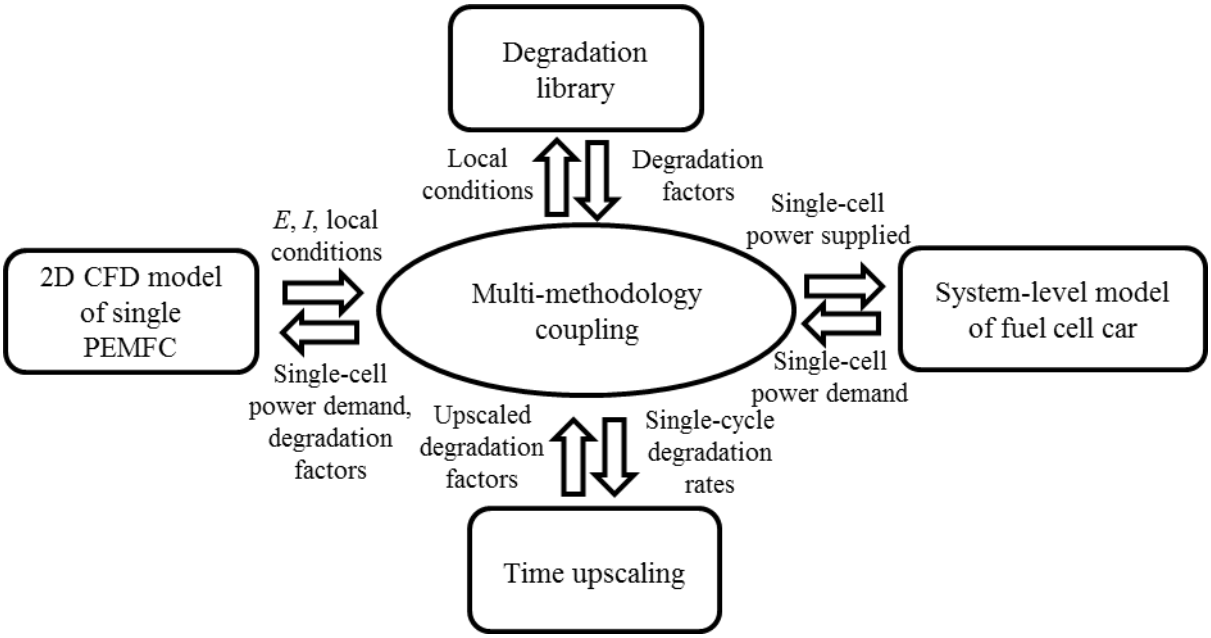

Figure 1: Schematic of the multi-methodology simulation framework.

The model is based on a number of key assumptions owing to the need to compromise between fidelity of the individual components and computational demand of the coupled framework:

- The car model assumes the PEMFC as only power sources (i.e., no hybridization).
- The fuel cell system is assumed to be represented by the single-cell channel-pair model. System components such as humidifiers, pressure control valves, heat exchangers, etc. are assumed ideal and are not explicitly modeled. As consequence, constant humidity is assumed in the fuel cell inlet gases.
- The single-cell model is assumed isothermal. Water transport is assumed single-phase (gas-phase) only.
- The membrane degradation is assumed to follow a simple mechanism used as an example to demonstrate the feasibility of the framework.

It is possible, and has of course been demonstrated by the respective disciplines, to relax these assumptions in more complex individual modeling approaches. Using high-end models of all components (car, fuel cell system, single cell, degradation), however, would render the multi-scale and multi-

methodology coupling computationally challenging and would additionally make results interpretation difficult. We therefore have limited the scope of the present paper to establish a basic yet flexible multi-timescale coupling that can be extended with other complementary component models, and demonstrate the feasibility of this model for predicting cell durability.

2.2 Virtual car model

The system-level model of the fuel cell car, which is implemented in Simulink, has various interacting modules that represent different subsystems of a car. Figure 2 shows a schematic of the virtual car subsystems and their interactions. Each of the modules is part of a control loop that attempts to match the velocity demand by assessing a corresponding power demand. The loop starts from a velocity input, which, for the present study, is taken from NEDC. However, the control framework can also work with other velocity profiles. The velocity demand (u_d) is sent to the engine controller, which, based on the current dynamics of the vehicle and state of fuel cell, requests required power ($P_{d,stack}$) from the fuel cell stack. The engine controller is a PI-controller with anti-windup correction [24] that attempts to match the current velocity of the vehicle supplied by the powertrain (u_s) to the velocity demand of the NEDC. The fuel cell stack downscales the stack power demand to cell level power demand ($P_{d,cell}$), which is the input to the single cell model (cf. section 2.2) that also includes an on-the fly cell degradation (cf. section 2.3). The power supplied ($P_{s,cell}$) by the fuel cell is upscaled by the fuel cell stack module ($P_{s,stack}$) and passed on to the electrical engine, which estimates the torque (τ) based on the current rotational speed (ω) of the engine (in revolutions per minutes, RPM) and power. Apart from the power generated from the NEDC requirements, we also set a constant auxiliary power demand of 400 W for the various non-power train components in the car (e.g. lights, stereo etc.). The power train block calculates the rotational speed of the engine (in RPM) and net expected driving force (F_D) on the vehicle, which finally is processed by the dynamics block to calculate the supplied velocity. The dynamics block works on the basic principles of Newtonian mechanics where the net inertial force is time-integrated to calculate the velocity.

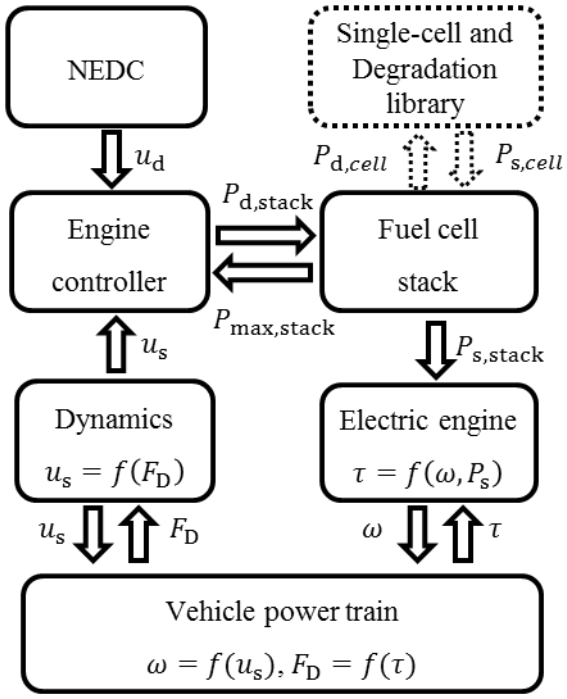

Figure 2: Schematic of the virtual fuel cell car.

Table 1 shows the model equations of the different vehicle subsystems. In order to use realistic parameters for the fuel cell car, we take typical values of a middle-sized passenger car [25], as given in Table 2. The fuel cell stack parameters are taken from the Auto-Stack project [26] and are also given Table 2.

Subsystem	**Governing equation**
Dynamics	Newton's law of motion $u_s = \int \frac{F_{\text{Inertial}}}{m_{\text{car}}} dt$ $F_{\text{Inertial}} = F_D - F_{\text{Drag}} - F_{\text{Rolling}}$ $F_{\text{Drag}} = \frac{c_w A \rho_{\text{air}} u}{2}$, $F_{\text{Rolling}} = C_r m_{\text{car}} g$
Power train	Transmission force

	$$F_{\mathrm{D}} = \eta_{\mathrm{gear}}\eta_{\mathrm{PT}}\frac{\tau}{R_{\mathrm{w}}}$$ Transmission RPM $$\omega = \eta_{\mathrm{gear}}\frac{u}{2\pi R_{\mathrm{w}}}$$
Electric engine	Electric motor torque equation $$\tau = \frac{P_{\mathrm{s}}}{\omega}$$
Engine controller	PI controller with anti-windup [24] $$P_{d,stack} = \begin{cases} K_p(u_d - u_s) + K_i \int (u_d - u_s)\, dt & if\ P_d < P_{max} \\ P_{max} & if\ P_d \geq P_{max} \end{cases}$$
Fuel cell stack	Stack power demand downscaling $$P_{\mathrm{d,cell}} = \frac{P_{\mathrm{d,stack}}}{N_{\mathrm{stack}}}$$ Single-cell power supply upscaling $$P_{\mathrm{s,stack}} = N_{\mathrm{stack}}P_{\mathrm{s,cell}}$$

Table 1: Model equations of the virtual car sub-systems. The parameter descriptions along with their values are given in the Table 2.

Parameter	**Value**
Mass of car + H_2 tank (m)	1100 kg + 99.7 kg[a]
Coefficient of rolling resistance (C_r)	0.0085[a]
Drag coefficient (C_w)	0.3[a]
Shadow area (A)	1.91 m^2[a]
Final drive ratio (η_{gear})	6.066[a]
Powertrain efficiency ($^{\eta}_{PT}$)	0.8[a]

Wheel radius (R_w)	0.291 m[a]
Auxiliary power consumption	400 W[a]
Fuel cell stack power	75 kW[c]
Number of cells in the stack (N_{stack})	315[b]
Cell area	0.03 m^2[b]
Total stack weight	153.8 kg[b]
Stack power density	0.49 kW/kg[c]
Proportional gain (K_p)	5[d]
Integrator gain (K_I)	0.6[d]

a : Estimated from a middle-size passenger car

b: Taken from Auto-Stack project [26]

c: Calculated from single cell performance

d: Tuned

Table 2: Virtual car and fuel cell stack parameters.

2.3 Single-cell multiphysics model

The single-cell model is a 2D CFD model based on Bao *et. al.* [22]. Figure 2 shows the computational geometry as implemented in COMSOL. It consists of two channels in counter-flow setup, two gas-diffusion layers, and the polymer membrane. The channel and GDL domains include multi-species transport. The cell operation is considered to be isothermal and the gases are considered to be ideal. Only vapor-phase transport of water is considered. The kinetics assumes modified Butler-Volmer equations based on elementary-kinetic mechanisms. The base model is described in detail in Ref. [22]. All model equations are given in Table 3, and model parameters are listed in Table 4. The base model is also modified to include lambda control with a minimum channel flow velocity ($u_{a,min}$, $u_{c,min}$) corresponding to reactant supply for a current density of 1000 A m^{-2}. The lambda-controlled velocity ensures a more efficient current density (load) based reactant supply. The idea of a minimum flow velocity is to ensure fast transient response by supplying sufficient reactants to the cell in an automotive

application while accelerating from an idling state. In order to simulate degradation, material properties that are assumed constant in the base model are modified over time according to relevant degradation mechanisms included the degradation library (cf. section below). For the present study, we particularly assume a temporal decrease in the membrane conductivity κ for demonstrating our cell durability prediction model. However, other material properties and transport coefficients can be (and will be in future work) integrated into the degradation library to achieve a robust durability prediction framework.

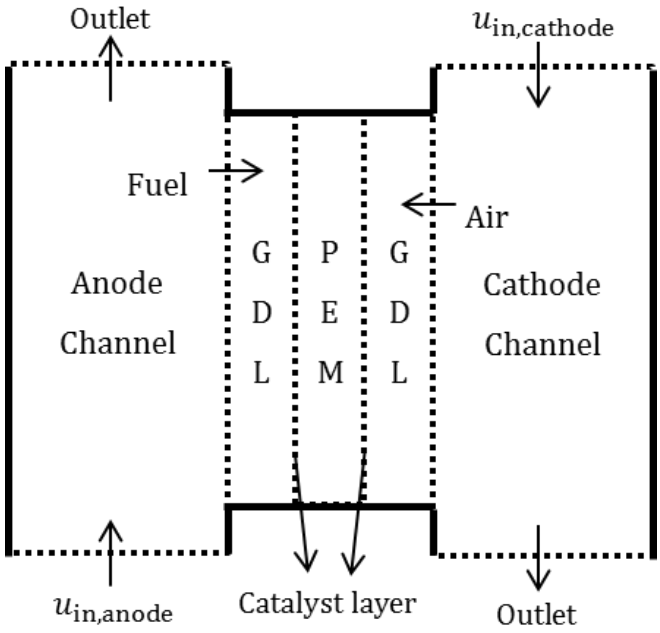

Figure 3: Two-dimensional computational domain of the single-cell model. Solid boundaries are no-flux boundaries. Not to scale.

Fuel cell component	**Equations**
Gas channels and GDLs	Mass and momentum transport equations $\frac{\partial(\varepsilon_p \rho)}{\partial t} + \boldsymbol{\nabla} \cdot (\rho \mathbf{u}) = 0$

	$$\frac{\rho}{\varepsilon_p}\left(\frac{\partial \mathbf{u}}{\partial t}+(\mathbf{u}\cdot\nabla)\frac{\boldsymbol{u}}{\varepsilon_p}\right)=\nabla\cdot\left[\left(-p\mathbf{I}+\frac{\mu}{\varepsilon_p}\left(\nabla\boldsymbol{u}+(\nabla\boldsymbol{u})^{\mathrm{T}}\right)-\frac{2}{3}\frac{\mu}{\varepsilon_p}(\nabla\cdot\boldsymbol{u})\right)\right]-\frac{\mu}{\mathrm{K}}\mathbf{u}+\mathbf{F}$$ Species mass balance $$\rho\varepsilon_p\frac{\partial \omega_i}{\partial t}+\nabla\cdot\mathbf{J}_i+\rho(\boldsymbol{u}\cdot\nabla)\omega_i=0$$ $$\mathbf{N}_i=\mathbf{J}_i+\rho\mathbf{u}\omega_i$$ $$\mathbf{J}_i=-\rho\omega_i\sum_k D_{ik,eff}\left[\nabla x_k+\frac{1}{p_A}(x_k-\omega_k)\nabla p_A\right]$$ $$x_k=\frac{\omega_k}{M_k}/\sum_i\frac{\omega_i}{M_i},\ \sum_i\omega_i=1$$ Lambda control $$u_{a,in}=\lambda_{fuel}\frac{RT_a i_{a,avg}L_{ch}}{2Fp_a x_{H_2,in}t_{ch}}+u_{a,min}$$ $$u_{c,in}=\lambda_{air}\frac{RT_c i_{c,avg}L_{ch}}{4Fp_c x_{O_2,in}t_{ch}}+u_{c,min}$$
Polymer Electrolyte Membrane (PEM)	Mass balance for protons $$\nabla\cdot\mathbf{N}_p=0$$ Mass balance for water $$\frac{1}{1+b\lambda}\frac{\rho_{m,dry}}{EW}\frac{d\lambda}{da_w}\frac{\partial a_w}{\partial t}+\nabla\cdot\mathbf{N}_w=0$$ Proton flux $$\mathbf{N}_p=-\kappa'\nabla\phi-\frac{\kappa'\xi}{F}\left[\frac{RT}{a_w}\nabla a_w+V_w\frac{\Delta p}{l_m}\mathbf{n}_y\right]-c_+\frac{k_{p,sat}}{\mu_{liq,w}}\frac{\lambda}{\lambda_{sat}}\frac{\Delta p}{l_m}\mathbf{n}_y$$ Water Flux $$\mathbf{N}_w=-\frac{\kappa'\xi}{F}\nabla\phi-\left(\frac{\lambda}{1+b\lambda}\frac{\rho_{m,dry}}{EW}\frac{D_{w,self}}{RT}+\frac{\kappa'\xi^2}{F^2}\right)\left[\frac{RT}{a_w}\nabla a_w+V_w\frac{\Delta p}{l_m}\mathbf{n}_y\right]$$ $$-\frac{\lambda}{1+b\lambda}\frac{\rho_{m,dry}}{EW}\frac{k_{p,sat}}{\mu_{liq,w}}\frac{\lambda}{\lambda_{sat}}\frac{\Delta p}{l_m}\mathbf{n}_y$$ Membrane conductivity degradation $$\kappa'=f_{deg}\kappa$$

Boundary conditions a) Between anode diffu-sion layer and PEM	Continuity of fluxes $\rho(\mathbf{u}\cdot\mathbf{n}) = \frac{\mathbf{N}_{\mathrm{H_2}}\cdot\mathbf{n}}{2F}\mathrm{M}_{\mathrm{H_2}} + \mathbf{N}_{\mathrm{H_2O}}\cdot\mathbf{n}\mathrm{M}_{\mathrm{H_2O}}$ $\mathbf{N}_{\mathrm{H_2}}\cdot\mathbf{n} = i_{\mathrm{a}}\mathrm{M}_{\mathrm{H_2}}/2\mathrm{F}$, $\mathbf{N}_{\mathrm{H_2O}}\cdot\mathbf{n} = (i_{\mathrm{a}}/2\mathrm{F} + N_{\mathrm{w}})\mathrm{M}_{\mathrm{H_2O}}$, $i_{\mathrm{a}} = \mathbf{N}_{\mathrm{p}}\cdot\boldsymbol{n} + C_{\mathrm{dl,a}}\frac{\partial\phi}{\partial t}$, $a_{\mathrm{w,a}} = p_{\mathrm{a}}x_{\mathrm{H_2O,a}}/p_{\mathrm{sat}}$, $\phi_a = 0$
b) Between cathode diffu-sion layer and PEM	Continuity of fluxes $\rho(\mathbf{u}\cdot\mathbf{n}) = \left(\mathbf{N}_{\mathrm{O_2}} + \mathbf{N}_{\mathrm{H_2O}}\right)\cdot\mathbf{n}$ $\mathbf{N}_{\mathrm{O_2}}\cdot\mathbf{n} = i_{\mathrm{c}}\mathrm{M}_{\mathrm{O_2}}/4\mathrm{F}$, $\mathbf{N}_{\mathrm{H_2O}}\cdot\mathbf{n} = (i_{\mathrm{c}}/2\mathrm{F} + N_{\mathrm{w}})\mathrm{M}_{\mathrm{H_2O}}$, $\boldsymbol{N}_p\cdot\boldsymbol{n} = i_{\mathrm{c}} - \mathrm{C}_{\mathrm{dl,c}}\frac{\partial\eta}{\partial t}$, $a_{\mathrm{w,c}} = p_{\mathrm{c}}x_{\mathrm{H_2O,c}}/p_{\mathrm{sat}}$ Modified Butler-Volmer equation $i_{\mathrm{c}} = \mathrm{i}_{0,353}\exp\left[\frac{\mathrm{E_{act}}}{\mathrm{R}}\left(\frac{1}{353} - \frac{1}{T}\right)\right]\left(\frac{p_{\mathrm{c}}x_{\mathrm{O_2}}}{\mathrm{RTc}_{\mathrm{O_2,ref}}}\right)^{\frac{(2-\beta_a)}{4}} a_{+}^{1-\beta_a}\left[\exp\left(-\frac{\beta_{\mathrm{a}}\mathrm{F}\eta}{\mathrm{RT}}\right) - \exp\left(\frac{(2-\beta_{\mathrm{a}})\mathrm{F}\eta}{\mathrm{RT}}\right)\right]$ $\eta = V_{cell} - \phi - V_{eq}$

Table 3: Governing equations for the single cell model. The symbols and their detailed meanings can be found in Bao *et. al.* [22].

Parameter	**Value**
MEA thickness (l_m)	50 μm[a]
PEM dry density ($\rho_{m,dry}$)	2000 kg/m^3 [a]
PEM swelling factor (b)	0.0126[a]
PEM saturated permeability ($k_{p,sat}$)	1.58x10^{-18} m^2 [a]
PEM saturated water uptake (λ_{sat})	14[a]

GDL thickness	300 μm[a]
GDL porosity (ε_p)	0.4[a]
GDL permeability (K)	10^{-11} m^{2} [a]
Channel width (t_{ch})	0.001 m[a]
Channel length (L_{ch})	0.9282 m[a]
Inlet gas pressure (p_c, p_a)	250 kPa
Flow mode	Counter-flow
Fuel stoichiometry (λ_{fuel})	1.3
Air stoichiometry (λ_{air})	1.5
Relative humidity	100% (Anode) 100% (Cathode)

[a] Taken from Bao *et. al.*[22]

Table 4: Single-cell parameters and operating conditions.

2.4 Degradation library

For a flexible integration of degradation models, a generalized component-wise degradation framework was developed. The main assumption of this framework is the decoupling of performance model and degradation model. Under this assumption, any multiphysics model parameter *P* (e.g., membrane conductivity or catalyst active area) can be represented as product of a performance function and a degradation factor,

$$P' = f_{P,\mathrm{deg}} \cdot P_{\mathrm{perf}} \tag{1}$$

where, P' is the parameter of the degraded cell, $f_{P,\mathrm{deg}}$ is the degradation factor which has values ranging from 1 (fresh cell) to 0 (completely degraded cell), and P_{perf} is the performance function. The degradation factor is calculated based on an appropriate degradation mechanism chosen from a degradation library, as described below. Both, the performance function and the degradation factor generally depend on local conditions (e.g., voltage, current density, species concentrations, temperature, etc.).

The approach of decoupling performance and degradation facilitates choice over various degradation and performance models through our modularized simulation framework. The approach is a first-order approximation towards the non-linear coupling between the current state of degradation and the performance model. The approximation can be justified by the fact that the performance functions have 'instantaneous' effect on the cell parameters while the degradation models take relatively longer time to reflect a significant change in them. This has been demonstrated in section 3.3. Moreover, the indirect nonlinear coupling between performance and degradation (or between different degradation mechanisms) is maintained via the functional dependence of both $f_{P,\mathrm{deg}}$ and P_{perf} on local state variables.

The degradation library (cf. Figure 1) is a collection of mathematical models that allows the calculation of degradation factors $f_{P,\mathrm{deg}}$ as a function of time and local conditions. Since, degradation and performance are assumed decoupled, the library can be modified, validated, used, and shared independently of the actual performance model. Specifically, the library contains models of local and instantaneous degradation rates ($\frac{\mathrm{d}f_{P,\mathrm{deg}}}{\mathrm{d}t}$) as function of local state variables (pressure, temperature, mole fractions, electric potentials),

$$\frac{\mathrm{d}f_{P,deg}}{\mathrm{d}t} = g(p, T, X_i, \phi) \quad . \tag{2}$$

The degradation function g can be generally derived from either experimental degradation measurements or lower-scale degradation models and can be given as look-up tables, analytical mappings, or fitted correlations. The current state of degradation of a cell property is calculated by time-integration of the local degradation rate,

$$f_{P,deg}(t + \Delta t) = f_{P,deg}(t) - \int_t^{t+\Delta t} \left(\frac{\mathrm{d}f_{P,deg}}{\mathrm{d}t}\right) \mathrm{d}t \quad . \tag{3}$$

In this study, the cell parameters and state variables are passed on to the degradation library that calculates the instantaneous rate of degradation from lookup tables and correlational mappings. The degradation rate is then time-integrated to obtain the change in the degradation factor over the numerical time step.

The goal of the present study is to demonstrate this framework and show its capability of end-of-life prediction studies under transient load conditions. To this end, we investigate the exemplary case of membrane degradation, i.e., loss of membrane conductivity κ. The membrane conductivity degradation is represented by a degradation factor ($f_{\kappa,deg}$) varying from 1 (for a fresh membrane) to 0 (for a completely degraded membrane) according to,

$$\kappa' = f_{\kappa,deg} \cdot \kappa(T,\lambda) \ , \tag{4}$$

where, Springer's expression [27] is used as the performance function for the conductivity as,

$$\kappa(T,\lambda) = (0.5139\lambda - 0.326) \cdot \exp\left[1268 \left(\frac{1}{303} - \frac{1}{T}\right)\right] \ . \tag{5}$$

For the present study we assume that the conductivity degradation rate linearly depends on the local O_2 partial pressure in the cathode catalyst layer. This assumption is based on the known complex membrane degradation mechanism [28] which is initiated by O_2 crossover from cathode to anode, which linearly depends on O_2 partial pressure. We furthermore assume that the membrane completely degrades within 5000 hours, which conforms to the durability targets of PEMFC stacks in transport applications [29]. We assume a degradation function based on a modest assumption that a 5000 h lifetime is reached under a steady-state operation with a fixed value of O_2 partial pressure ($p_{\mathrm{O_2,steady}}$) representative of air operation at open circuit, 80 °C, 2.5kPa, and 100 % RH. This leads to the degradation function,

$$\frac{\mathrm{d}f_{\kappa,deg}}{\mathrm{d}t} = g(p, X_i) = \frac{p_{\mathrm{O}_2}}{5000 \cdot p_{\mathrm{O}_2,\mathrm{steady}}} hour^{-1} \,. \tag{6}$$

This is certainly a simplified description of membrane degradation, which nevertheless allows to fully represent the coupling between the multiphysics performance model and the degradation library, and therefore demonstrating the utility of present framework for durability predictions. It is out of the scope of this study to develop a detailed membrane degradation model, which will be the subject of future investigations.

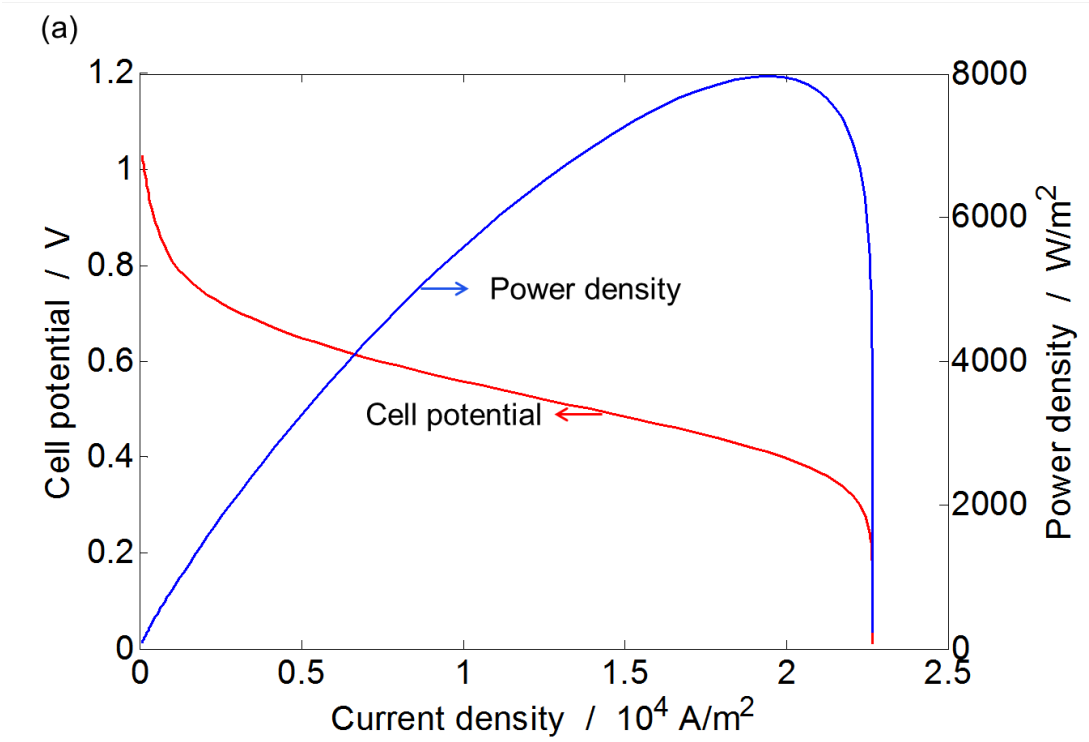

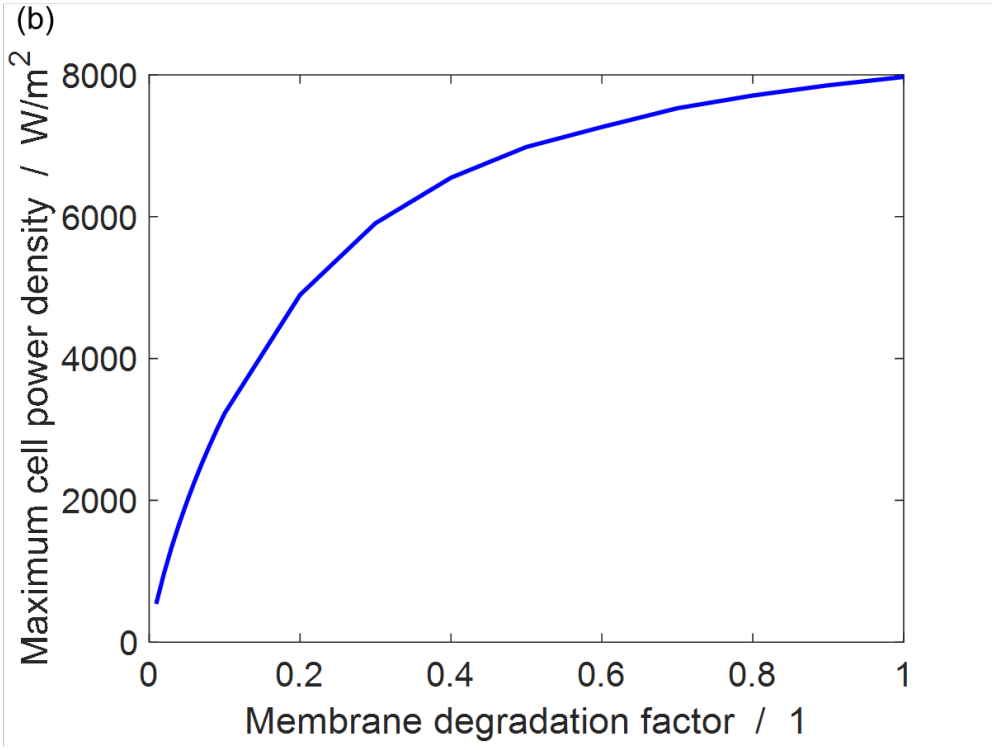

Figure 4. (a) Simulated *I-V* curve of the single-cell model without degradation.(b) Maximum power output of the single cell model under different states of membrane degradation.

Figure 4a shows simulated *V-I* and *P-I* curves under base conditions, that is, non-degraded cell (Table 4). Figure 4b shows the maximum power density delivered by a single cell as a function of the membrane degradation factor. The fuel cell performance shows a nonlinear dependence on the degradation factor, with significant performance loss only for $f_{\kappa,\mathrm{deg}} < 0.5$. This shows that the membrane resistance does not dominantly contribute to the overpotentials under base conditions (i.e., full humidification). Moreover, Figure 4b also helps to estimate the cell end-of-life under a certain load cycle. For example, under the considered stack size, cell area, and car parameters in this study, NEDC requires a maximum single cell power density of 4011 W m^{-2}. This suggests that at a membrane degradation factor value of approximately 0.15, the cell will fail to deliver the required power.

2.5 End-of-life cell durability prediction

One of the advantages of PEMFC modeling is that it provides a time- and cost-effective predictive analysis of cell durability under extended end-of-life loading cycles. Cell degradation over one NEDC, which is only approx. 20 minutes long, is not significant enough to predict the cell behavior over a

stack life of 5000 hours owing to the non-linear coupling between cell electrochemistry and degradation processes. Moreover, as a fully coupled 2D spatio-temporally resolved CFD simulation of PEMFC under a highly transient loading is not real-time capable, it is not feasible to simulate the entire time duration of 5000 hours. Therefore, in order to allow for long-term cell degradation predictions, we developed a piecewise (two-step) time-upscaling methodology. In this methodology, we start with a non-degraded cell (i.e. the value of the degradation factor is 1). We simulate the cell behavior under the transient power demand of one complete NEDC. The cell's state of degradation (represented by the degradation factor) is calculated by integrating the instantaneous degradation rate ($\mathrm{d}f_{P,deg}/\mathrm{d}t$) over the NEDC duration. Next, this degradation factor is linearly upscaled over a time period of n NEDCs to extrapolate the state of degradation of the cell. With the extrapolated value of the degradation factor, the n+1st NEDC is simulated, and the mentioned two-step cycle is repeated. The entire process is continued until the degrading fuel cell fails to provide the necessary power to run one complete NEDC. The time-upscaled degradation factor is calculated as,

$$f_{P,deg}(t + n \cdot t_{NEDC}) = f_{P,deg}(t) - n \cdot \int_{t}^{t+t_{NEDC}} \frac{df_{P,deg}}{dt} dt \quad , \tag{7}$$

where, n is the number of NEDC upscaling cycles (here $n = 1000$ cycles which is equivalent to 328 hours and 11023 km), and t_{NEDC} is the time duration of one NEDC (1180 seconds). Although, the time-upscaling is linear, the methodology captures the long-term nonlinearity of degradation through the non-linear variation in the degradation rate over every n+1st driving cycle.

2.6 Multi-platform coupling and simulation technology

The current simulation platform takes advantage of the individual strengths of the simulation platforms such as MATLAB, Simulink and COMSOL. The system-level car model is implemented in Simulink, while the multiphysics single-cell model is implemented in COMSOL. We use MATLAB as an interface between these codes. The communication between MATLAB and COMSOL is established with the help of a MATLAB S-function and COMSOL Livelink. The degradation library consists of a collection of MATLAB functions. Although every individual component (cell, system, degradation) has its own dynamics, all components are directly coupled ("horizontal" or "on-the-fly" cou-

pling) and multiscale transient simulations are carried out at component level. The overall model input is a velocity profile that in this study is the NEDC.

Simulink uses a Bogacki-Shampine solver with fixed time-step of 0.2 s. COMSOL uses backward differentiation formula (BDF) solver, which is a variable order, variable time-step solver. All simulations were performed on an Intel quad-core processor with a base frequency of 3.4GHz and 16 GB RAM. Wall-clock time is approximately 30 hours for simulating one complete NEDC.

3 Results and discussions

3.1 Power cycle

The objective of the virtual car model is to convert the velocity cycle data to fuel-cell-relevant power cycle data, which can be used as a power demand from the fuel cell system. Figure 5 shows the power demand generated by the car controller corresponding to the NEDC based velocity cycle and the velocity supplied by the car dynamics block. One can observe that the maximum power requirement from the fuel cell stack for the given values of car parameters over the NEDC is approximately 39 kW.

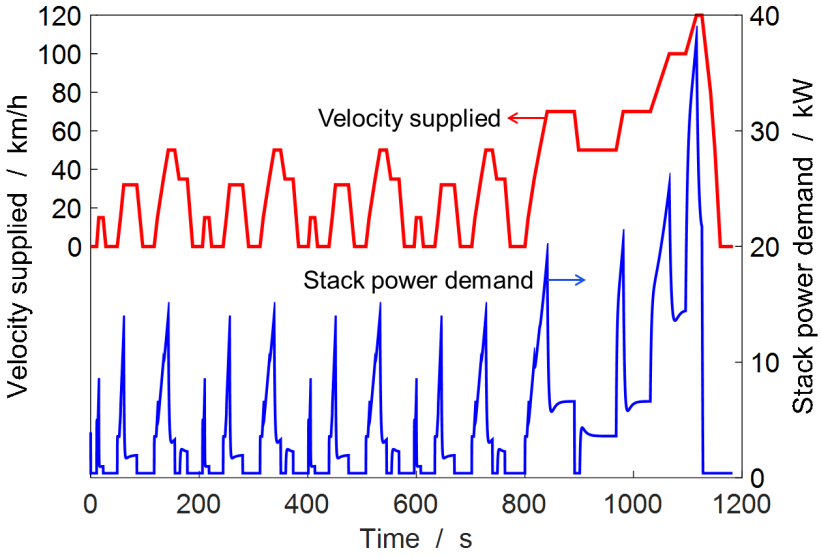

Figure 5: Simulated vehicle velocity and stack power demand corresponding to the NEDC, using the virtual fuel cell car model.

3.2 Single-cell performance

With the help of the previously-mentioned multiscale coupled simulation framework, the single-cell performance can be simulated during an NEDC with respect to various operating conditions. Figure 6 shows simulated single-cell current and voltage during one driving cycle. The highly transient power demand causes a highly transient current density and voltage behavior. From the cell voltage and current density transience, it can be observed that the fuel cell response closely follows the transient power demand. It can also be observed that with the current stack size, the fuel cell operates within the cell voltage range of 1.05 V-0.62 V between idling and peak power demand. The cell efficiency using, $\eta_{fuel\ cell} = \frac{V}{1.25} \times 100\%$, in the given voltage range of 1.05- 0.62 V is 84-49.6%.

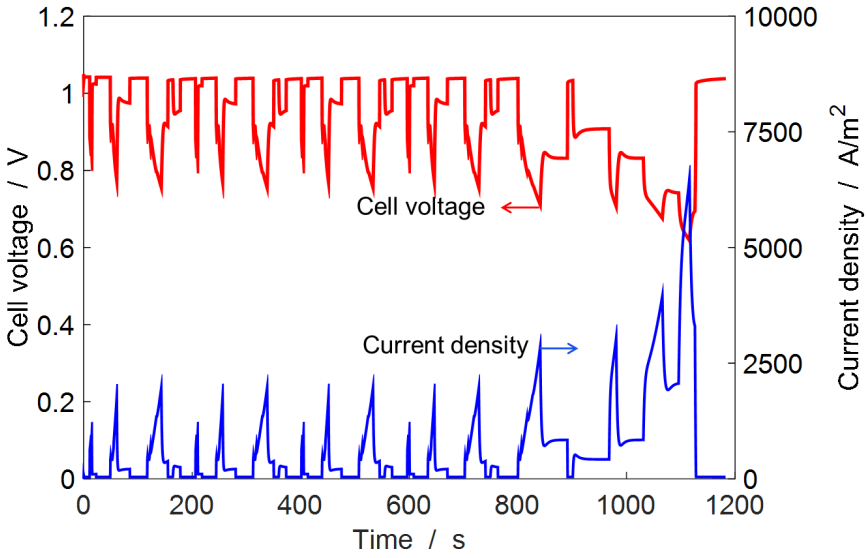

Figure 6: Cell potential and current density variation in a single cell during the NEDC.

One of the challenges in fuel cell operation is water management, which greatly affects the performance of PEM fuel cells. The water management in PEM fuel cells can be categorized into two broad contexts, firstly, membrane hydration, which is important for proton conductivity in the membrane and secondly, cathode flooding, which might hamper diffusion of reactants into the catalyst layer. Within the scope of this study, we will be focusing only on the membrane hydration, as assumed cell operating conditions are not conducive to the cathode flooding situation and also due to limited scope of this study regarding two-phase flow and transport in the GDL. Further, due to the isothermal nature of this model, we have not considered the changes in the relative humidity due to the variations in the cell

operating temperature. Also, we have considered an ideal supply of homogeneously humidified gases at the channel inlets. Moreover, it has to be noted that membrane water content not only affects the fuel cell performance but also affects the membrane longevity through various mechanical and chemical degradation mechanisms [2]. Figure 7 shows a spatial average of the membrane water content λ as function of time over two consecutive simulated NEDCs and at two different values of pre-humidification of the fuel and air. The transient cell operation also results in a transient variation in the membrane water content. The membrane water content strongly depends on the pre-humidification of the inlet gases. At higher values of pre-humidification (RH_c = RH_a = 100%), the membrane is always fully saturated ($\lambda_{avg} > 14$ [27]), while at lower values of pre-humidification (RH_c = 30 %, RH_a = 50 %), the membrane hardly attains saturation. The range of λ is considerably smaller in the case of high humidification compared to low humidification Also, when comparing two consecutive NEDCs with respect to the membrane water uptake (λ_{avg}), one can see that the difference between initial state of λ_{avg} for the two consecutive NEDCs is a strong function of the operating conditions. Such an observation is useful for the present study where the objective is to use a representative NEDC for time-upscaling simulations to predict cell durability. So, in order to demonstrate our fuel cell durability framework in the present work, we chose the relative humidity of 100% in both anode and cathode channels.

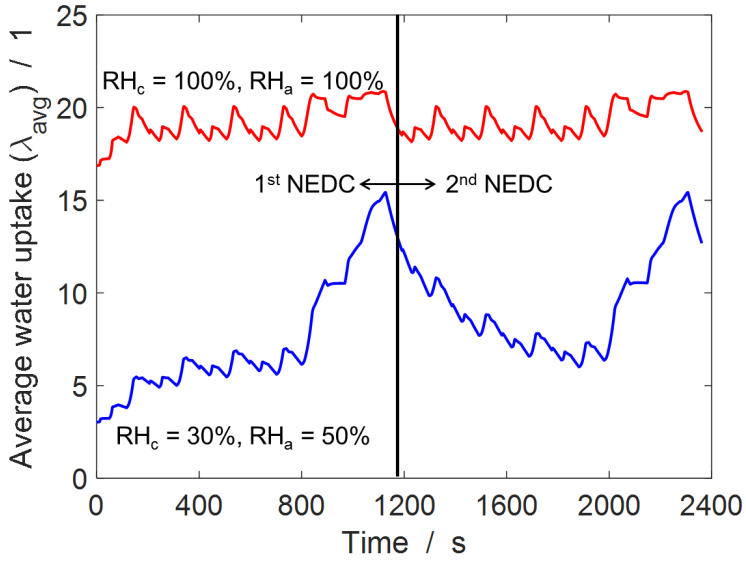

Figure 7: Spatially averaged water uptake (λ_{avg}) in the membrane at different relative inlet humidities over a duration of two consecutive NEDCs. The two consecutive NEDCs are separated by a black line.

An important parameter affecting the water uptake of the membrane is the partial pressure of water vapor in the GDLs. The magnitude of the partial pressure of water vapor governs whether the water vapor will condense into liquid or the existing liquid water will evaporate. Figure 8 shows spatiotemporally resolved simulation results of water vapor partial pressure at the catalyst layers along the channel length during the NEDC. Assumed inlet humidifications are 100% RH. The saturation water vapor pressure at 80℃ is around 47 kPa which is more than the maximum observed partial pressure in cathode. This means that under the assumed conditions, the water vapor will not condense into liquid water and hence less cathode flooding is expected. The highly transient cycling of local water vapor concentration observed at the cathode and anode GDLs can be detrimental to the mechanical stability of the membrane. This may lead to mechanical degradation by stressing of the membrane due to a swelling and shrinkage cycling because of the changes in the membrane water content, eventually changing the membrane structural properties [30]. Since, the present study assumes a cross-flow configuration (fluid flow direction marked by arrows in the figure), one can also observe that the highest water vapor presence is consistently near the inlet section of anode and outlet of the cathode. This means that the channel inlets are exposed to higher concentrations with slower transience as compared to the center of the channel. A relatively persistent presence of water vapor means that those locations in the membrane are exposed to less cycling and hence less mechanical damage occurs in those locations. But at the same time, they expose the membrane to a more steady chemical damage [30].

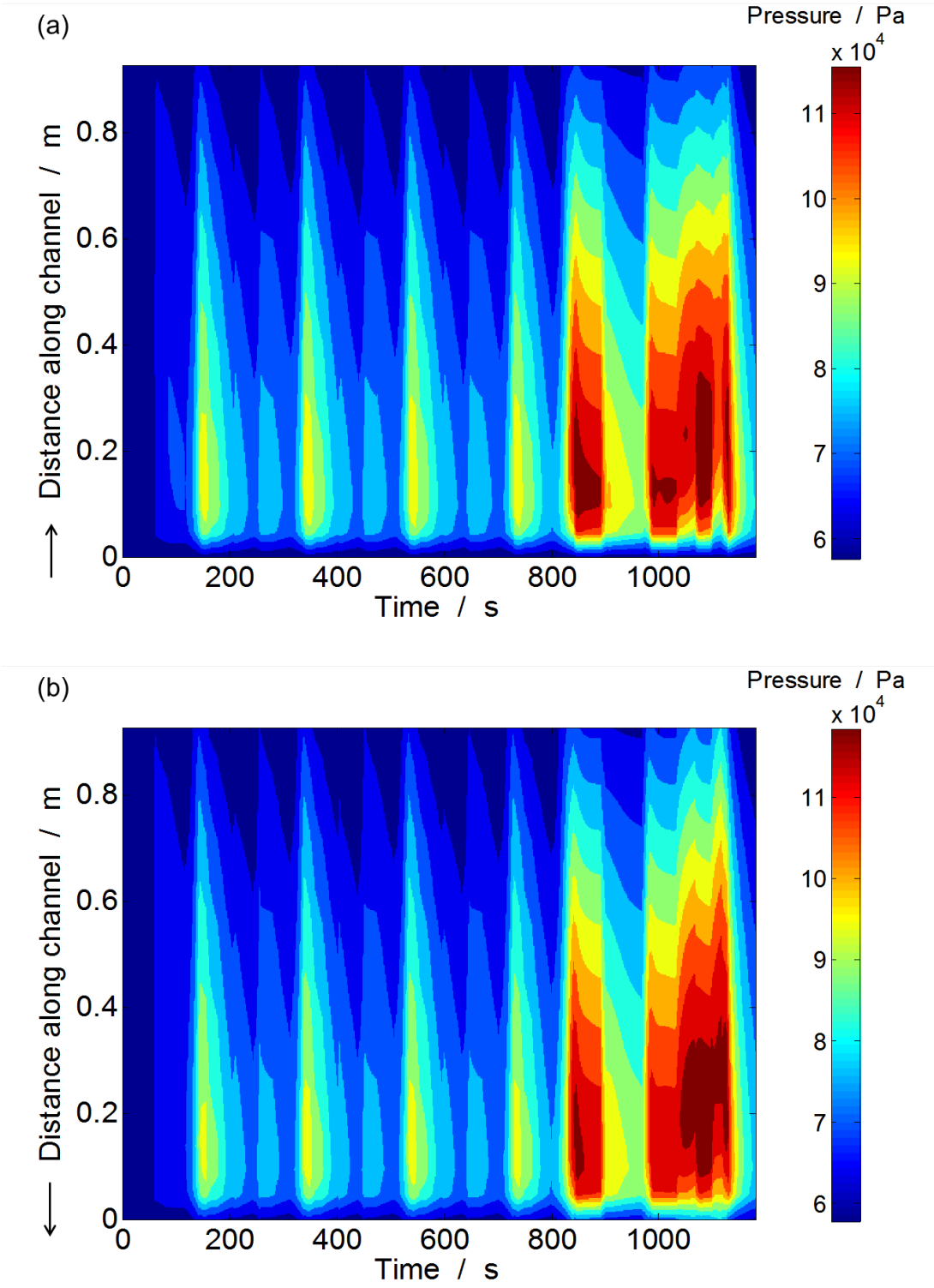

Figure 8: $H_2O_{(g)}$ partial pressure distribution at (a) anode and (b) cathode catalyst layer as function of time and spatial position along channel length over one NEDC for inlet humidification of 100%. The arrow shows the direction of the imposed flow.

Figure 9 shows the spatio-temporal distribution of H_2 and O_2 partial pressures in anode and cathode

catalyst layer, respectively, for the same simulation case. Here, we can see that for the assumed counter-flow configuration, the H_2 concentration decreases quickly near the anode channel entrance, while, O_2 concentration decreases near the exit of the cathode channel. This demonstrates that the maximum reaction kinetics occurs at the above locations with a significant spatial variation along the channel length. This also explains the maximum water vapor concentration at those locations. Moreover, the locations along the channel with higher partial pressures of the reactants, i.e., anode exit for H_2 and cathode entrance for O_2, are more prone to gas crossovers. Such a spatially distributed presence of membrane degradation mechanisms such as humidity cycling, chemical degradation, and gas crossovers, demonstrates that membranes undergo a distributed state of degradation and subsequently highlights the need for a multidimensional modeling study like this for cell degradation analysis.

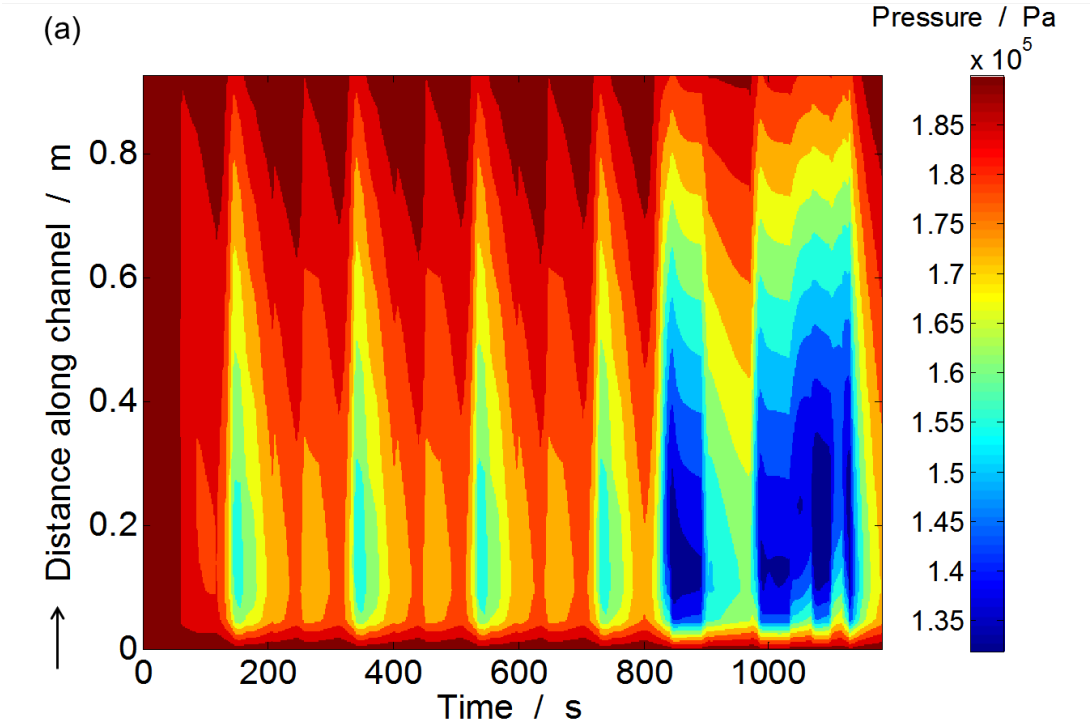

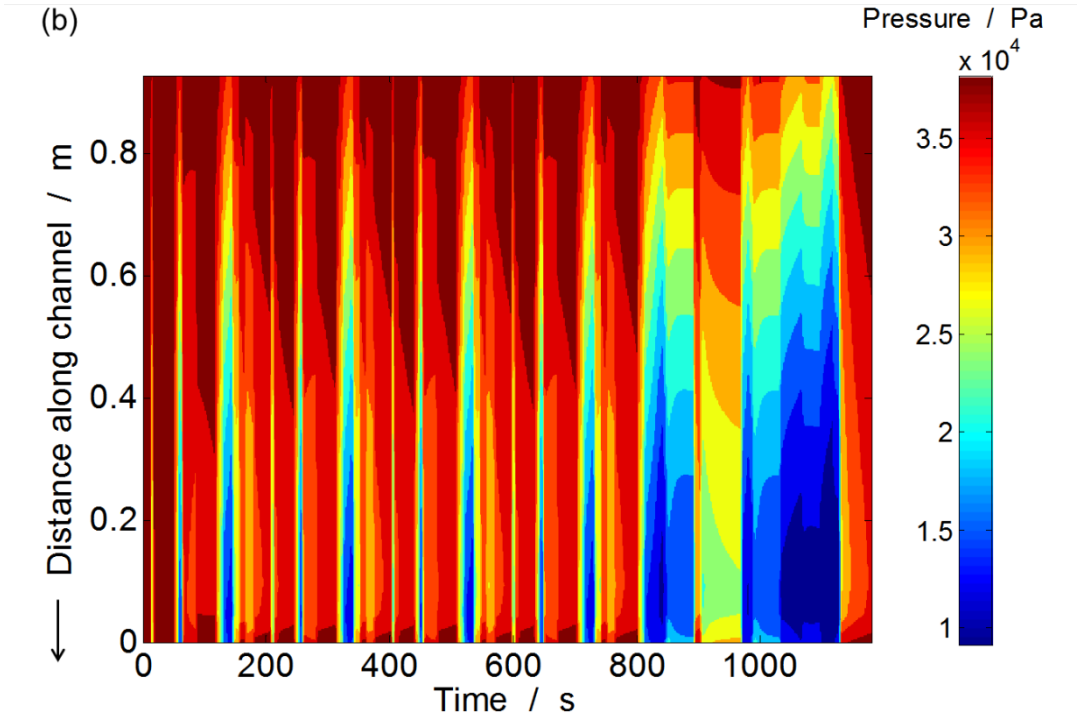

Figure 9: Partial pressure distribution of (a) fuel (H_2) and (b) oxidant (O_2) in anode and cathode catalyst layer, respectively, as function of time and spatial position along channel length over one NEDC for inlet humidification of 100%. The arrow shows the direction of the imposed flow.

3.3 End-of-life cell durability simulations

Using the degradation framework mentioned in section 2.3 and time-upscaling methodology discussed in section 2.4, a PEMFC under membrane conductivity degradation was simulated for 20000 NEDCs (corresponding to 6555 hours). Results of this study are shown in Figure 10 and Figure 11. Figure 10a) shows the simulated degradation rate as function of time for NEDC numbers 1 and 20001. The strong variations in the rate of degradation show that under the transient load cycling, the cell state variables also show a highly sensitive transience that eventually influence the local degradation rate. This is a result of the simplistic membrane degradation model used for the present demonstration. Figure 10b) shows the variation in the spatially averaged membrane conductivity over time-upscaled NEDCs. The results demonstrate the performance model induced short-term (several seconds time scale) and degradation model induced long-term (several thousand hours time-scale) variations in the membrane conductivity. The observed short-term variation in the conductivity over one NEDC is due to the local

variation in the water uptake in the membrane due to the current density transience. The results also show significant reduction in the membrane conductivity towards the cell end-of-life.

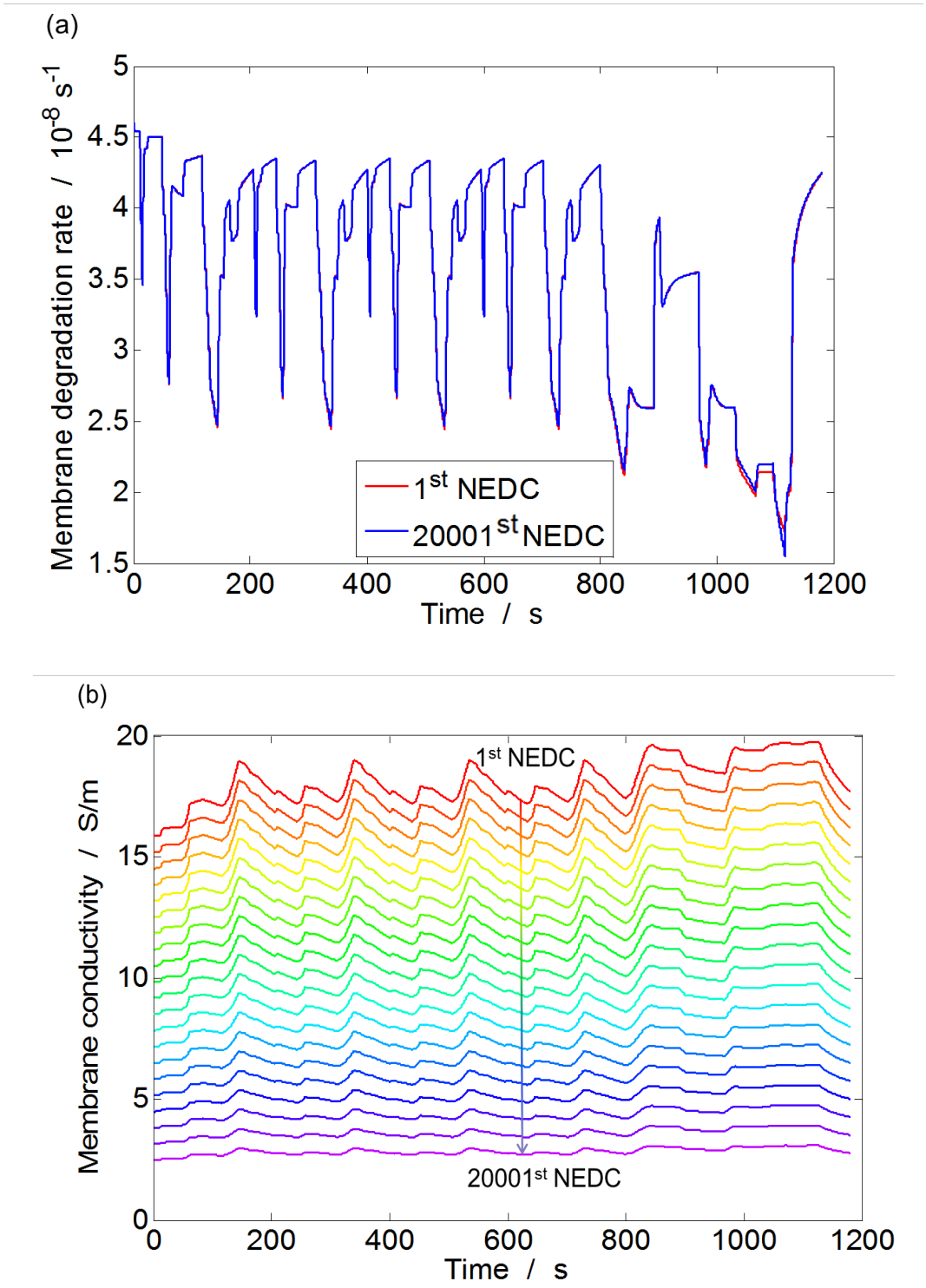

Figure 10: (a) Variation in membrane degradation rate during the first NEDC and after 20000 NEDCs, (b) membrane conductivity variation during one complete NEDC and for various upscaled states of degradation each after 1000 NEDC jumps.

Figure 11a) shows the reduction in the membrane degradation factor over time. As discussed in Section 2.3, one can estimate the cell end-of-life from the state of membrane degradation, which was estimated at a degradation factor value of around 0.15. As shown in the figure, the cell achieved the mentioned end-of-life criterion after about 20000 NEDCs. This translates to a timespan of approximately 6555 hours and a distance of 220,500 km. Such a fuel cell stack life exceeds the expected 5000 hours stack life in a fuel cell powered vehicle.

Figure 11b) shows the reduction of cell voltage and increase in current density at an NEDC time of 1116 s (cf. Figure 7), which corresponds to the maximum power demand region from the highway section of the NEDC. The loss of cell performance can be associated with the decrease in the cell voltage that after 20000 NEDCs reduces by approximately 172 mV, thus significantly reducing the cell efficiency. The reduction in cell voltage is generally used as a reference for durability criterion. To put things in perspective, for catalyst degradation in automotive applications, the expected reduction in cell voltage over 5000 hours is 30 mV [31].

The quasi-linear decrease in the degradation factor with time as shown in Figure 11a) can be attributed to the fact that the underlying degradation rate is assumed to be a function of the partial pressure of oxygen, which has a consistent supply over the cell lifetime. Further, although there is a significant variation in the degradation during a driving cycle, multiple exposures to such load cycling has relatively insignificant change in the degradation rates during the cell lifetime (cf. Fig. 10a). However, the reduction in membrane conductivity has a nonlinear effect on the transport of protons through the transport equations (cf. Table 3). This consequently explains the observed nonlinear decrease in cell performance in Fig. 11b.

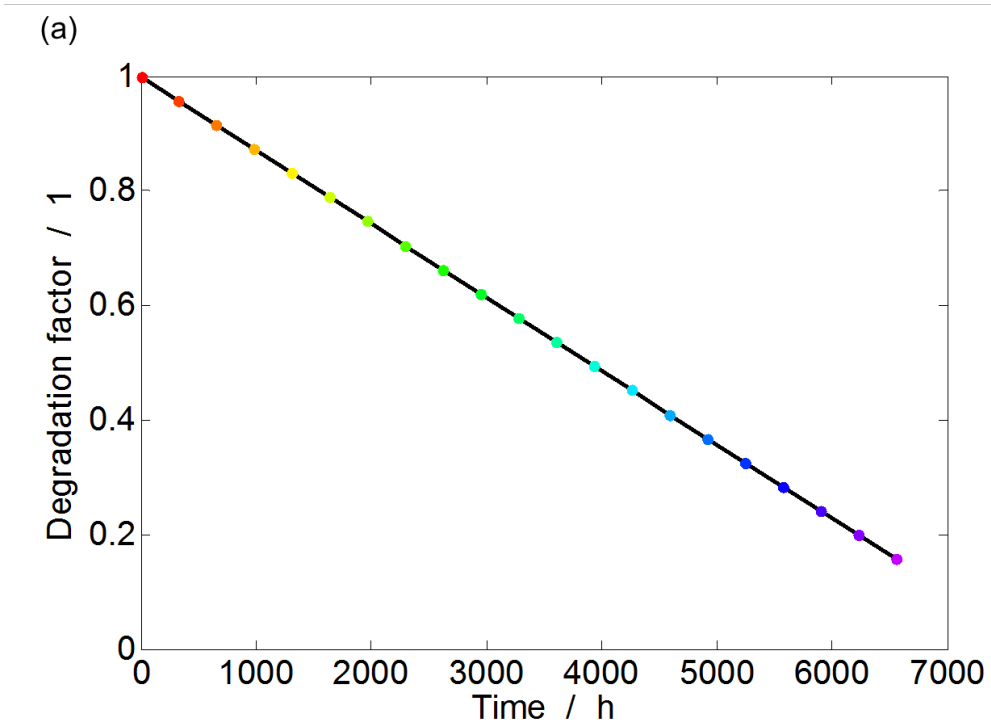

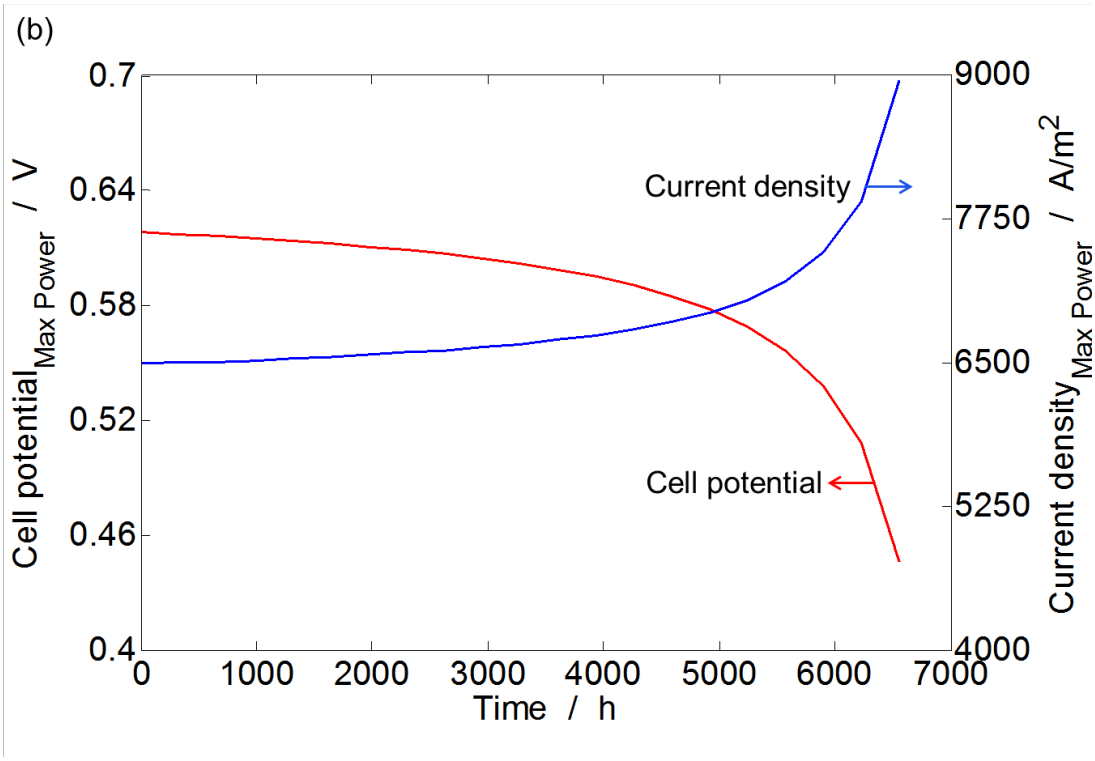

Figure 11: (a) Reduction in membrane degradation factor with time, where the colored dots correspond to the respective colored NEDC jump from the Figure 10b), and (b) cell potential and current density corresponding to the maximum power demand (NEDC time 1116 s) under time-upscaled membrane conductivity degradation model.

It should be noted that the results presented in this section are based on a simple membrane degrada-

tion model which is linear with respect to local partial pressure of O_2. This allows to demonstrate the multi-methodology approach developed here, while still providing qualitatively meaningful results. Future work will be devoted to including extended physically-based degradation mechanisms in the degradation library for quantitative end-of-life analysis.

4 Conclusions

We have presented the development and demonstration of a multiscale computational framework that couples a detailed 2D cell-level model of a PEM fuel cell with a system level virtual car model. We have demonstrated that with such a multiscale coupling, we can obtain real-time local state variables as a function of global operating conditions, which are instrumental for reliably predicting cell life-time. To this goal, the simulation framework is able to flexibly accommodate degradation mechanisms based on lower-scale physical processes with real-time feedback of fuel cell state variables. The mathematical decoupling of performance and degradation allows for the establishment of a flexible degradation library that can include correlations, look-up tables or analytical mappings. With the help of a time-upscaling approach, the computational framework can describe cell parameter variations over three different time scales, (1) sub-second timescale of electrochemistry, (2) minute-timescale of driving cycles, and (3) thousand-hour-timescale of degradation. We have demonstrated an end-of-life durability analysis of the fuel cell due to membrane degradation under a highly transient loading of the New European Driving Cycle.

In the present study we did not include a secondary energy storage device (e.g., a lithium-ion battery) into the virtual car. This setup was chosen in order to identify critical cell loading regions imposed by the NEDC operation and consequently propose relevant degradation mitigation schemes. Yet, the present simulation framework is able to accommodate on-board secondary energy storage systems, the influence of which will be investigated in future work. A key assumption of the present work is the simple membrane degradation mechanism. Future work will implement detailed physically-based degradation mechanisms, taking advantage of the flexible degradation library.

5 Acknowledgements

The research leading to this work has been supported by the European Union's Seventh Framework

Program for the Fuel Cells and Hydrogen Joint Technology Initiative under the project PUMA MIND (grant agreement no 303419).

6 References

1. P. Corbo, F. Migliardini, and O. Veneri, *Hydrogen fuel cells for road vehicles* (Springer, 2011).
2. M. M. Mench, E. C. Kumbur, and T. N. Veziroglu, *Polymer electrolyte fuel cell degradation* (Academic Press, 2012).
3. C. C. Chan, "The State of the Art of Electric, Hybrid, and Fuel Cell Vehicles," Proc. IEEE **95**, 704–718 (2007).
4. L. Gao, Z. Jiang, and R. A. Dougal, "An actively controlled fuel cell/battery hybrid to meet pulsed power demands," J. Power Sources **130**, 202–207 (2004).
5. P. Thounthong, S. Raël, and B. Davat, "Energy management of fuel cell/battery/supercapacitor hybrid power source for vehicle applications," J. Power Sources **193**, 376–385 (2009).
6. P. Thounthong, S. Raël, and B. Davat, "Control strategy of fuel cell/supercapacitors hybrid power sources for electric vehicle," J. Power Sources **158**, 806–814 (2006).
7. S. Eaves and J. Eaves, "A cost comparison of fuel-cell and battery electric vehicles," Journal of Power Sources **130**, 208–212 (2004).
8. R. Borup, J. Meyers, B. Pivovar, Y. S. Kim, R. Mukundan, N. Garland, D. Myers, M. Wilson, F. Garzon, D. Wood, P. Zelenay, K. More, K. Stroh, T. Zawodzinski, J. Boncella, J. E. McGrath, M. Inaba, K. Miyatake, M. Hori, K. Ota, Z. Ogumi, S. Miyata, A. Nishikata, Z. Siroma, Y. Uchimoto, K. Yasuda, K.-I. Kimijima, and N. Iwashita, "Scientific aspects of polymer electrolyte fuel cell durability and degradation," Chemical reviews **107**, 3904–3951 (2007).
9. P. T. Yu, W. Gu, R. Makharia, F. T. Wagner, and H. A. Gasteiger, "The Impact of Carbon Stability on PEM Fuel Cell Startup and Shutdown Voltage Degradation," ECS Trans. **3**, 797–809 (2006).
10. J. Wu, X. Z. Yuan, J. J. Martin, H. Wang, J. Zhang, J. Shen, S. Wu, and W. Merida, "A review of PEM fuel cell durability: Degradation mechanisms and mitigation strategies," J. Power Sources **184**, 104–119 (2008).
11. X. Cheng, Z. Shi, N. Glass, L. Zhang, J. Zhang, D. Song, Z.-S. Liu, H. Wang, and J. Shen, "A review of PEM hydrogen fuel cell contamination: Impacts, mechanisms, and mitigation," Journal of Power Sources **165**, 739–756 (2007).
12. A. A. Franco, "Multiscale modelling and numerical simulation of rechargeable lithium ion batteries: concepts, methods and challenges," RSC Adv. **3**, 13027 (2013).
13. A. A. Franco, ed., *Polymer electrolyte fuel cells*. Science, applications, and challenges (Pan Stanford, 2013).

14. W. G. Bessler, “Multi-scale modelling of solid oxide fuel cells,” in *Solid Oxide Fuel Cells: From Materials to System Modeling*, M. Ni and T. S. Zhao, eds. (Royal Society of Chemistry, 2013), pp. 219–246.
15. A. Schell, H. Peng, D. Tran, E. Stamos, C. C. Lin, and M. J. Kim, “Modelling and control strategy development for fuel cell electric vehicles,” Annual Reviews in Control **29**, 159–168 (2005).
16. C. N. Maxoulis, D. N. Tsinoglou, and G. C. Koltsakis, “Modeling of automotive fuel cell operation in driving cycles,” Energy Conversion and Management **45**, 559–573 (2004).
17. A. Veziroglu and R. Macario, “Fuel cell vehicles: State of the art with economic and environmental concerns,” International Journal of Hydrogen Energy **36**, 25–43 (2011).
18. P. Ekdunge and M. Raberg, “The fuel cell vehicle analysis of energy use, emissions and cost,” International Journal of Hydrogen Energy **23**, 381–385 (1998).
19. D. D. Boettner, G. Paganelli, Y. G. Guezennec, G. Rizzoni, and M. J. Moran, “Proton Exchange Membrane Fuel Cell System Model for Automotive Vehicle Simulation and Control,” J. Energy Resour. Technol. **124**, 20 (2002).
20. J. Pukrushpan, A. Stefanopoulou, and H. Peng, *Control of fuel cell systems* (Springer, 2005).
21. K. H. Hauer and R. M. Moore, “Fuel Cell Vehicle Simulation– Part 3. Modeling of Individual Components and Integration into the Overall Vehicle Model,” Fuel Cells **3**, 105–121 (2003).
22. C. Bao and W. G. Bessler, “Two-dimensional modeling of a polymer electrolyte membrane fuel cell with long flow channel. Part I. Model development,” Journal of Power Sources **275**, 922–934 (2015).
23. E/ECE/TRANS/505/Rev.2/Add.100/Rev.3, *Agreement concerning the adoption of uniform technical prescriptions for wheeled vehicles, equipment and parts which can be fitted and/or be used on wheeled vehicles and the conditions for reciprocal recognition of approvals granted on the basis of these prescriptions* (2013).
24. K. J. Åström and T. Hägglund, *PID controllers*, 2nd ed. (International Society for Measurement and Control, 1995).
25. M. Roche and N. Artal, “Evaluation of Fuel Cell Vehicle regarding Hybridization Degree and its impact on Range, Weight and Energy Consumption,” in *European Electric Vehicle Congress*. *3-5 December* (2014).
26. A. Martin and L. Joerissen, “Auto-Stack - Implementing a European Automotive Fuel Cell Stack Cluster,” in *2011 Fuel Cell Seminar & Exposition*, ECS Transactions (ECS, 2012), pp. 31–38.
27. T. E. Springer, T. A. Zawodzinski, and S. Gottesfeld, “Polymer Electrolyte Fuel Cell Model,” J. Electrochem. Soc. **138**, 2334 (1991).
28. W. Schmittinger and A. Vahidi, “A review of the main parameters influencing long-term performance and durability of PEM fuel cells,” Journal of Power Sources **180**, 1–14 (2008).
29. US Department of Energy, *Table II: Technical targets fir membranes: Automotive* , http://energy.gov/eere/fuelcells/downloads/table-ii-technical-targets-membranes-automotive.

30. D. E. Curtin, R. D. Lousenberg, T. J. Henry, P. C. Tangeman, and M. E. Tisack, “Advanced materials for improved PEMFC performance and life,” Journal of Power Sources **131**, 41–48 (2004).
31. A. Ohma, K. Shinohara, A. Iiyama, T. Yoshida, and A. Daimaru, “Membrane and Catalyst Performance Targets for Automotive Fuel Cells by FCCJ Membrane, Catalyst, MEA WG,” ECS Trans. **41**, 775–784 (2011).